

On Learning-Assisted Content-Based Secure Image Transmission for Delay-Aware Systems with Randomly-Distributed Eavesdroppers — Extended Version —

Mehdi Letafati, *Student Member, IEEE*, Hamid Behroozi, *Member, IEEE*, Babak Hossein Khalaj, *Senior Member, IEEE*, and Eduard A. Jorswieck, *Fellow, IEEE*,

Abstract

In this paper, a learning-aided content-based wireless image transmission scheme is proposed, where a multi-antenna-aided source wishes to securely deliver an image to a legitimate destination in the presence of randomly distributed eavesdroppers (Eves). We take into account the fact that not all regions of an image have the same importance from the security perspective. Hence, we propose a transmission scheme, where the source employs a hybrid method to realize both the error-free data delivery of public regions—containing less-important pixels; and an artificial noise (AN)-aided transmission scheme to provide security for the regions containing large amount of information. Moreover, in order to reinforce system's security, fountain-based packet delivery is adopted: First, the source node encodes image packets into fountain-like packets prior to sending them over the air. The secrecy of our proposed scheme will be achieved if the legitimate destination correctly receives the entire image source packets, while conforming to the latency limits of the system, before Eves can obtain the important regions. Accordingly, the secrecy performance of our scheme is characterized by deriving the closed-form expression for the quality-of-security (QoSec) violation probability. Moreover, our proposed wireless image delivery scheme leverages the deep neural network (DNN) and learns to maintain optimized transmission parameters, while achieving a low QoSec violation probability. Simulation results are provided with some useful engineering insights which illustrate that our proposed learning-assisted

M. Letafati, H. Behroozi, and B. H. Khalaj are with the Department of Electrical Engineering, Sharif University of Technology, Tehran 1365-11155, Iran (e-mails: mletafati@ee.sharif.edu; behroozi@sharif.edu; khalaj@sharif.edu). E. A. Jorswieck is with the Department of Information Theory and Communication Systems, TU Braunschweig, Germany (e-mail: e.jorswieck@tu-bs.de).

scheme outperforms the state-of-the-arts by achieving considerable gains in terms of security and the delay requirement.

Index Terms

Content-aware security, wireless image transmission, learning-aided secure communication, delay-aware packet delivery.

I. INTRODUCTION

The modern era of wireless communication is facing a remarkable evolution that has led to the development of beyond-the-fifth-generation (B5G) mobile technologies, which assert supporting an overabundance of contemporary services including the Internet-of-Things (IoT), autonomous driving, and Augmented/Virtual Reality (AR/VR) [1]. Meanwhile, comprehensive studies are being conducted on the sixth generation (6G) of wireless cellular systems to look for its potential development challenges [2].

Despite the genuinely-designed networking protocols of 5G and B5G communication systems, security challenges are still witnessed as open issues that have not been thoroughly addressed. Simultaneously, on the roadmap towards 6G, new security challenges can be identified due to the considerable revisions of key communication parameters and operational entities, e.g., the end-to-end tolerable latency; the deployment of long-lasting IoT devices with security requirement; the wide-range usage of different RF technologies; and, the quantum computers [2], [3].

A. Motivation

Although a great amount of innovative studies have been carried out on the security of the 5G core network [4], the wireless edge of 5G, B5G, and also 6G systems is vastly encountered with ever-rising attacks, e.g., jamming, eavesdropping, and traffic analysis, which can be deployed at a low price, using low-cost software defined radios. More precisely, the intrinsic broadcast nature of wireless medium has made the wireless networks susceptible to security and privacy risks [5].

In this regard, physical layer security (PLS) solutions, which leverage intrinsic properties of the radio channel, can be incorporated thanks to their inherent capability of being adapted to the communication medium [3], [5], [6]. The main idea of PLS is to make the legitimate link better than the unauthorized links of potential adversaries. Remarkably, a great number of new

attributes of future networks, such as low-latency control systems and sensor fusions, require only localized communications, where the core network is not engaged. Hence, utilizing PLS approaches can provide a desirable level of agile security for such scenarios. In addition to rendering flexible secure frameworks, PLS can achieve information-theoretic security guarantees via utilizing lightweight mechanisms [7].

Remarkably, owing to the ability of machine learning (ML)-based techniques to acquire and learn complex features of data, utilizing ML can help PLS solutions propel the secrecy performance of wireless systems to a state that reliable context-aware security can be achieved with a low computational complexity [3]. For instance, the secrecy of wireless communications can be enhanced via utilizing deep neural networks (DNNs) to intelligently maintain optimal transmission parameters [8], [9].

Recently, wireless image transmission, as a practical scenario of reliable data delivery, is receiving much attention from both academia and industry, due to its applications in newly-emerged services such as AR/VR or surveillance systems [10]. In this regard, if the transmitted images are not rigorously secured, the performance of such wireless services are no longer reliable. Moreover, from the quality of service (QoS) point of view, the delay imposed to the imaging systems due to the transmission of large-sized images should be handled properly. Conventional wireless image transmission schemes were realized through computationally expensive cryptographic methods or digital watermarking techniques [11], which are easily breakable with the increasing growth in the computational capabilities of modern computers, e.g., quantum computing technology. Therefore, the PLS-based approaches together with ML techniques can be leveraged to provide flexible delay- and content-aware security solutions for wireless image delivery.

B. Related Works

A large number of researches in the PLS domain has been carried out to study the so-called secrecy capacity (SC), which is defined as the maximum data rate that can be reliably and confidentially transmitted, e.g., in some case, the difference between the capacities of the main and wiretap channels to provide perfect secrecy [12]–[14]. However, the SC-inspired transmission design dictates a much lower acceptable data rate, which may result in large delivery delays. Despite the growing demand for higher capacities, the emergence of the IoT-enabled services is imposing a paradigm shift from the capacity-centric mobile services towards reliable delay-aware

and content-based services. Accordingly, in a practical scenario of wireless image transmissions, the perfect secrecy is not realizable [15]–[18]. In other words, from the view-point of an eavesdropping adversary, the original image cannot be retrieved even if a small number of packets are correctly received.

In the area of PLS-based data delivery, the authors in [15] examined an adaptive allocation of physical resources in a fountain coding (FC)-aided point-to-point (P2P) system of delivering medical images. A similar single-input single-output (SISO) FC-assisted wireless network was examined in [16] and [17] with more emphasis on the image content and the channel imperfections, respectively. The FC as a low-complexity technique has been shown to be able to improve packet delivery security at the physical layer (PHY) [19]. In fountain-coded transmissions, the original data is first divided into a series of, e.g., N , source packets, which are then linearly combined to obtain encoded packets. The source message can be entirely recovered at receiver, iff at least N independent FC packets are successfully received [19]. Remarkably, despite addressing the delay limits of a practical system in [15]–[17], the researchers did not provide a *closed-form expression* for their performance metric. The FC-aided packet delivery was applied to cooperative networks in [18], by deploying more complex techniques in addition to FC, i.e., cooperative jamming and relay selection. However, the researchers’ proposed scheme in [18] did not take the content of transmitted data into account, yielding an unconscious packet delivery scheme. Moreover, a fixed rate transmission was considered in their work regardless of wisely considering the link quality and the content of image. Notably, all of the studies mentioned above, considered only one single-antenna eavesdropper (Eve) in their model, where some partial information regarding the wiretap channel is available.

C. Contributions

In this paper, different from [15]–[19], we investigate a multi-input single-output (MISO) FC-aided wireless system, where a multi-antenna source node aims to send an image to a legitimate destination, while conforming to the acceptable delay limits of delivering the file. In addition to the legitimate entities, different from [7], [12]–[19], in our proposed system model we assume *multiple totally passive* randomly-located Eves which are trying to wiretap the wireless image delivery. The eavesdroppers in our system model are assumed to be distributed according to homogeneous Poisson point process (PPP) [24]. We also consider both cases of non-colluding eavesdropping (NCE) and colluding eavesdropping (CE) scenarios throughout our

analysis and results. Moreover, it is considered in our system model that we have an uncertain (imperfect) estimation regarding the legitimate link, while there is no channel state information (CSI) available at the legitimate source about the eavesdropping links.

We address the content of the image through the process of secure wireless transmission in the sense that not all regions of an image have equal importance levels from the content-centric view. Accordingly, we consider the image to be partitioned into two segments, i.e., the region of interest (RoI) and the background (BG), where the RoI source packets of an image are likely to contain important diagnostic information regarding the content of an image. Hence, the RoI packets will require stringent security and reliability specifications, while the BG packets do not provide useful data if being revealed to the passive Eves. Remarkably, a content-based secure wireless image delivery is not addressed in many recently-published works in the area of wireless image transmission, e.g., [10], [20], [21]. In other words, they all consider a unified end-to-end approach for sending an image over the air, regardless of paying attention to the content/region of the image being transmitted at each transmission slot (TS). In contrast, we propose a hybrid transmission policy according to the type of the source packets scheduled to be transmitted. When sending RoI-related packets, our proposed system model deploys maximum ratio transmission (MRT) beamforming together with artificial noise (AN) injection, as a practical and low cost PLS technique [22], to achieve a physical enhancement for the legitimate link, while degrading the eavesdropping ability of potential Eves. For the transmission of BG packets, we simply deploy MRT in order to save power consumption and improve the packet accumulation ability of legitimate receiver, since the BG regions require less stringent security. We also stress that in order to reinforce the system's capability for reliable transmission of image source file, our proposed scheme also exploits FC and encodes the original source packets into fountain-like packets prior to MRT deployment.

In this paper, different from the previous works of [7], [12]–[14], and [21], we take the delay limits of a practical image transmission system into account via utilizing a hybrid multi-packet transmission design. We then derive an exact closed-form expression, which was not obtained in [15]–[17], for the quality-of-security (QoSec) violating probability (QVP) as our performance metric to address the effect of delay limits on the image delivery. The QVP metric characterizes the performance of our system to correctly recover the entire image at destination before Eves can obtain the RoI-related important regions, while conforming to the delivery delay limits.

In our proposed model, we further formulate an optimization problem opted for reducing the

QVP by maintaining optimal transmission parameters. Due to the non-linear characteristics of our objective and constraints, finding optimal solutions through conventional algorithms may result in low efficiency and long delay effect in a practical deployment. Therefore, we utilize a DNN composed of dense layers as our learning-based approach to provide an efficient and flexible method of finding optimal transmission parameters. In other words, we exploit the potential of DNN in intelligently adjusting our image transmission scheme to minimize the QVP performance metric, which was not considered in [12]–[18]. By leveraging the DNN, we perform an offline phase of data set generation for numerous realizations of the wireless medium. Our developed DNN then learns an optimum mapping between the generated realizations and the associated optimal policies. Afterwards, our trained DNN provides approximate performance for new realizations of the network via a significantly-low computational complexity that actually corresponds to performing a forward propagation through the trained DNN online. Finally, our simulation results clearly illustrate the performance of our proposed learning-based delay-aware scheme compared with the state-of-the-art benchmarks for image transmission.

The remainder of this paper is orchestrated as follows. In Section II, our proposed system model together with the main assumptions and intuitions are provided. Section III proposes our transmission policy for secure wireless image delivery. In Section IV, we investigate the performance of our proposed scheme through deriving closed-form expression of the QVP. The details on how to obtain optimal transmission parameters for the ML aspect of our proposed scheme are studied in Section V. In Section VI, extensive simulation results are provided to verify the analytical results. We also compare our learning-based scheme with different benchmarks and baselines. Section VII concludes the paper and presents useful insights for further research directions.

Notations: We denote the transpose, the conjugate transpose, and ℓ^2 norm of a vector by $(\cdot)^T$, $(\cdot)^\dagger$, and $\|\cdot\|$, respectively. Moreover, $|\cdot|$ represents the absolute value of a scalar variable and the cardinality of a set. Vectors are represented by bold lowercase letters, while matrices are written as bold uppercase symbols. $\mathcal{CN}(\mu, \sigma^2)$, $\text{Exp}(\lambda)$, and $\mathcal{G}(N, \lambda)$ represent a complex random variable (RV) with mean μ and variance σ^2 , exponential distribution with parameter λ , and gamma distribution with parameters N and λ , respectively. The expected value, the probability density function (pdf) (also the probability mass function (PMF) for a discrete RV), the cumulative distribution function (CDF), and the complementary cumulative distribution function (CCDF) of RV X are denoted by $\mathbb{E}[X]$, $f_X(x)$, $F_X(x)$, and $\overline{F}_X(x)$, respectively. Moreover, the probability of

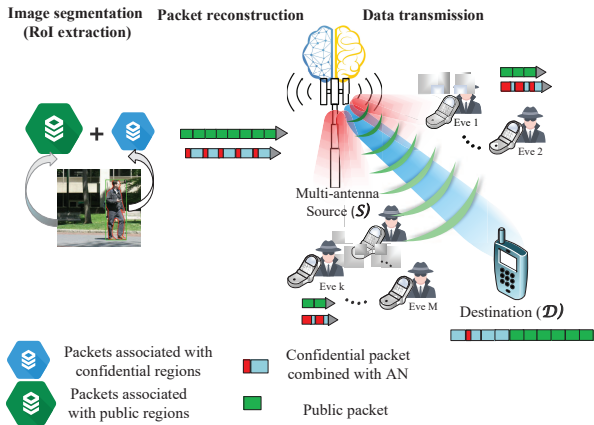


Fig. 1: Proposed Learning-assisted System Model for Packet-based Wireless Image Transmission.

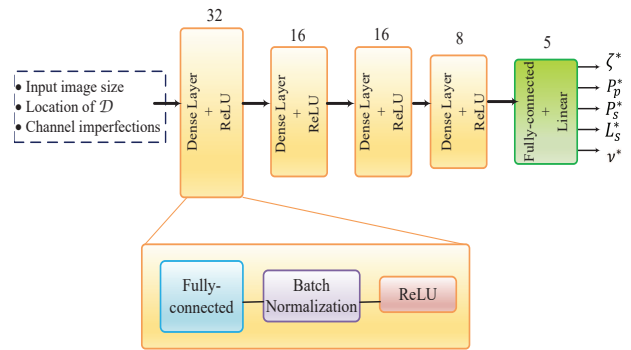


Fig. 2: Our proposed DNN for content-aware wireless image transmission. The number of neurons in each layer is shown at the top of that layer.

an event A is denoted by $\Pr(A)$. $W_{\nu,\mu}(x)$, $\Gamma(x)$, $B(m, n)$, and $\gamma(\alpha, \beta)$ are the Whittaker function [33, Eq. (9.22)], the Gamma function [33, Eq. (8.31)], the Beta function [33, Eq. (8.384)], and the lower incomplete Gamma function [33, Eq. (8.350)], respectively.

II. SYSTEM MODEL

Consider a MISO wireless image transmission system, where the source node \mathcal{S} , equipped with n_T transmit antennas, delivers an image file to a single-antenna legitimate destination node \mathcal{D} , as depicted in Fig. 1. Due to broadcast properties of wireless medium, the transmission is concurrently overheard by randomly distributed single-antenna *totally-passive* eavesdroppers (Eves), where the locations of Eves are modeled as a homogeneous PPP Φ_E of density λ_E on a 2-D plane with the i -th Eve at distance r_i ($i \in \Phi_E$) from \mathcal{S} . We consider two eavesdropping strategies for the existing Eves in our proposed model, i.e., the NCE case, where the wiretap capacity is determined by the maximum capacity among all \mathcal{S} -to-Eves links; and the CE case, in which Eves cooperate with each other to improving their ability of wiretapping image delivery. Without loss of generality, we presume \mathcal{S} to be placed at the origin and \mathcal{D} at a known position with distance r_D from \mathcal{S} . In other words, the source node is fully aware of the legitimate destination's position, while presumes a probabilistic model for the location of passive Eves.

To deliver the image source file, \mathcal{S} first splits the file into N source packets denoted by $\{\pi_1, \pi_2, \dots, \pi_N\}$, each containing the same number b of bits. The source packets will further be transformed into a potentially unlimited number of fountain-based coded packets. Each coded packet is obtained by XORing a subset of the source packets. More details about fountain-

based packet reconstruction will be mentioned later. During each TS, one or several fountain packets form the transmit frame with duration T at PHY which is then sent out over the wireless channel. The available bandwidth for each slot is B Hz. At the end of any time slot, the legitimate receiver \mathcal{D} , as well as Eves, performs channel decoding on the received signals. Successfully-received packets are acknowledged by sending an ACK packet through a feedback channel from \mathcal{D} to \mathcal{S} . The feedback signals, do not contain any information regarding the original image. The transmission is terminated when \mathcal{D} gathers N independent fountain-based coded packets to decode the entire original source file or the delay limit arrives. To guarantee image delivery security, the number of independent fountain-encoded packets collected at Eves should be less than N at the time of delivery termination; In addition, the Eves should not obtain any useful information corresponding to sensitive (confidential) regions of an image, e.g., the details of someone's face in a secrecy-assuring transmission.¹

In this paper, we take into account the fact that not all regions of an image have the same importance level from the security/content perspective. For instance, the RoI packets tend to contain the highest portion of information regarding the source image; hence, they need a higher security and reliability requirement. On the contrary, the BG regions of an image, in most cases, do not contain any useful information about the targeted image. Accordingly, we propose a hybrid transmission method for the delivery of source packets based on their type to ensure a reliable and secure transmission for the entire image file. More specifically, the source image is first divided into two parts: the confidential packets, related to the RoI, which is subject to security constraints and tends to contain the highest portion of information about the entire image; and the public part, namely the background (BG), which can be sent over the air with less stringent security limits, since revealing it to potential Eves does not leak any useful data. Notably, this segmentation can be realized via utilizing threshold-based image saliency detection methods [16].² Mathematically speaking, at \mathcal{S} 's side and after segmenting the source image, extracted packets form two disjoint sets: Π_s , corresponding to packets with security constraints; and Π_p , corresponding to public BG packets, respectively, where $\Pi_s \cap \Pi_p = \emptyset$, $|\Pi_s| = N_{\text{roi}}$, and $|\Pi_p| = N_{\text{bg}} = N - N_{\text{roi}}$. N_{roi} and N_{bg} respectively denote the number of RoI and BG packets. The two sets of $|\Pi_s|$ and $|\Pi_p|$ are illustrated, respectively, by blue and green stacks in Fig. 1.

¹The operational meaning of this measure is comprehensively studied in Section IV of our paper.

²Investigating different methods of image segmentation is out of the scope of this article.

At each TS, \mathcal{S} estimates its legitimate link's condition; determines which kind of packet to be sent; and provides appropriate resource for transmission. Remarkably, a trained DNN is developed at the source node which is opted for facilitating the procedure of choosing the best transmission parameters. The details on how to train and utilize the DNN deployed at \mathcal{S} will be discussed later. Selected source packets are then encoded to form a transmitting frame. If the confidential packets are selected to form the frame, coded packets are further combined with AN, shown by red data packets in Fig. 1, to ensure secrecy for the confidential packets $\{\pi | \pi \in \Pi_s\}$. The frame is then sent over the wireless medium by exploiting MRT beamforming (together with the injected AN, if a confidential region is going to be transmitted). At the receiving end, both \mathcal{D} and Eves attempt to gather sufficient number of packets to recover the source image.

All wireless channels are assumed to undergo quasi-static flat-fading with a large-scale path loss exponent $\eta > 2$, where the channel coefficients remain constant during each time slot and vary independently among different slots. Also, the channel coefficients of different links are independent of each other. The channel vector from \mathcal{S} to a node j with a distance r_j is characterized as $\mathbf{h}_{sj}r_j^{-\frac{\eta}{2}}$, where $\mathbf{h}_{sj} \in \mathbb{C}^{n_T \times 1}$ denotes the small-scale fading vector, with independent and identically distributed (i.i.d.) elements $h_{sj,i} \sim \mathcal{CN}(0, 1)$. In order to obtain an estimation regarding the quality of the legitimate link at \mathcal{S} , the destination node sends pilot signals at the beginning of each TS, and $\hat{\mathbf{h}}_{sd}$ is obtained at \mathcal{S} [23]. In this paper, we assume imperfect channel acquisition at legitimate nodes. Accordingly, the fading vector of the exact main channel from \mathcal{S} to \mathcal{D} , denoted by \mathbf{h}_{sd} , is different from $\hat{\mathbf{h}}_{sd}$ due to imperfect channel reciprocity caused by the outdated CSI [23]. Hence, the fading vector of main channel is modeled as

$$\mathbf{h}_{sd} = \rho \hat{\mathbf{h}}_{sd} + \sqrt{1 - \rho^2} \hat{\mathbf{e}}_{sd}, \quad (1)$$

where $\hat{\mathbf{e}}_{sd}$ reflects the uncertain part of $\hat{\mathbf{h}}_{sd}$ with i.i.d. entries $\hat{e}_{sd,i} \sim \mathcal{CN}(0, 1)$. Moreover, $\rho \in (0, 1)$ denotes the correlation coefficient between \mathbf{h}_{sd} and $\hat{\mathbf{h}}_{sd}$, which can easily be calculated from the knowledge of wireless medium parameters [23]. We also define $\hat{g}_{sd} \triangleq \|\hat{\mathbf{h}}_{sd}\|^2$ as the estimated channel gain of the legitimate \mathcal{S} -to- \mathcal{D} link, where the estimation is done by \mathcal{S} . We also assume that the CSIs of \mathcal{S} -to-Eves are unknown. Without loss of generality, we assume that the noise n_j at each node j is statistically independent additive white Gaussian noise (AWGN) and follows $\mathcal{CN}(0, \sigma_n)$.

III. DESIGN OF THE TRANSMISSION SCHEME

In this section, we present a detailed description of our proposed image transmission scheme, including the strategies for fountain-encoding of source packets, transmit frame reconstruction, and the signaling design of our proposed semi-adaptive transmission. Prior to image delivery, the source file is firstly divided into N source packets corresponding to N non-overlapping regions. The extracted source packets are then partitioned into two sets of secure (RoI-related) packets, Π_s , and public ones, denoted by Π_p .

Without loss of generality, we consider the file delivery during arbitrary slots of $t - 1$ and t . We also emphasize that the allowable delay limit for the image delivery to take place is D_{lim} . Therefore, we have $t \leq D_{lim}$. In the t -th TS, in order to construct a transmitting data frame, \mathcal{S} estimates the instantaneous gain $\hat{g}_{sd}(t)$ to obtain an estimate about the quality of legitimate link. Hereafter, if the instantaneous gain $\hat{g}_{sd}(t)$ exceeds a threshold ν , indicating a sufficiently good link quality, confidential packets corresponding to RoI regions are called to construct transmit frame. Otherwise, the transmitting frame will comprise public packets [15]. Next step is to establish the semi-adaptive transmission strategy. That is, if the public packets are selected to construct the frame, an adaptive number of packets (denoted by L_p) which are aimed to be transmitted during the t -th slot is derived. Calculation of L_p is done in a way that ensures all L_p packets can be decoded by \mathcal{D} successfully. On the other hand, if the confidential packets are called for transmission, a fixed rate R_s (bits per channel use) is set at \mathcal{S} , and $L_s = \frac{R_s}{b}$ packets from Π_s are pre-processed to be sent over the air. Instructions for calculating appropriate L_p and R_s are studied in detail during later sections. In order to enhance the level of security for the packet-based transmission scheme, the raw selected source packets are further encoded into fountain-like packets in the application layer before designing the transmitting signal at PHY [17], [18]. This is elaborated in the following subsection.

A. Fountain-like Packet Reconstruction

According to the feedback of \mathcal{D} to \mathcal{S} during slots 1 to $t - 1$ and the fountain-like encoding rule which is publicly shared among system nodes, \mathcal{S} updates two sets for each of the public and confidential packets, i.e., a recovered set \mathcal{R}_k , and an unrecovered set \mathcal{U}_k , $k \in \{s, p\}$, which are, respectively, composed of all the source packets that have been and have not been recovered at \mathcal{D} , by the t -th slot. Without loss of generality, we consider \mathcal{U}_k has the form $\mathcal{U}_k = \{\pi_1^k, \pi_2^k, \dots, \pi_{|\mathcal{U}_k|}^k\}$, for $k \in \{s, p\}$. In time-slot t , considering $L_p < |\mathcal{U}_p|$ (if public packets are scheduled to

be transmitted) or $|\mathcal{U}_s| > L_s$ (otherwise), \mathcal{S} calls the most recently recovered source packet $\pi_{\text{rec}}^k \in \mathcal{R}_k$ and XORs it with L_k unrecovered source packets $\{\pi_{\text{ind}}^k, \dots, \pi_{\text{ind}+L_k-1}^k\}$ from \mathcal{U}_k to generate L_k fountain-encoded packets, where ind denotes the starting index of chosen packets. Mathematically speaking, we have the following encoding strategies to obtain a coded packet denoted by c_l at the application layer

$$c_l = \begin{cases} \pi_{\text{rec}}^{\text{p}} \oplus \pi_{\text{ind}+l}^{\text{p}}, & \text{for } 0 \leq l \leq L_p - 1, \quad \text{if } \Psi_0 \\ \pi_{\text{rec}}^{\text{s}} \oplus \pi_{\text{ind}+l}^{\text{s}}, & \text{for } 0 \leq l \leq L_s - 1, \quad \text{if } \Psi_1 \end{cases} \quad (2)$$

where Ψ_0 and Ψ_1 correspond to the case of public and confidential data transmission, respectively. Equivalently, Ψ_0 corresponds to the case of $\hat{g}_{sd} \leq \nu$, while Ψ_1 corresponds to complementary case of $\hat{g}_{sd} > \nu$, with

$$\Pr(\Psi_1) \stackrel{(a)}{=} 1 - \Pr(\Psi_0) = e^{-\nu} \sum_{i=0}^{n_{\text{T}}-1} \nu^i / i!, \quad (3)$$

which follows directly from the fact that $\hat{g}_{sd} \triangleq \|\hat{\mathbf{h}}_{sd}\|^2$ obeys Gamma distribution $\mathcal{G}(n_{\text{T}}, 1)$ [32]. We also note that if $L_p(L_s) \geq |\mathcal{U}_p|(|\mathcal{U}_s|)$, all source packets in $\mathcal{U}_p(\mathcal{U}_s)$ are selected to generate fountain-coded packets similar to (2).

By invoking (2) and considering the fact that the fountain-coded packets will be sent over the wireless channel (which is discussed in the next subsection), since the \mathcal{S} -to-Eves channels vary independently compared to the legitimate link, it is unlikely for Eves to be able to decode exactly the same packet(s) as \mathcal{D} does. Hence, missing a frame at any Eve, means the linear combination of source packet(s) included in that frame may never be seen by her again.

Remark 1: To further exploit the content of the image file opted to be transmitted in a delay-limited scenario, the source packets can be prioritized in a pre-processing step, according to their content. Toward this end, pixels with higher saliency values or the ones having edge contents can be considered to have higher levels of importance for the legitimate observer. In this regard, a practical method for determining the level of importance for each source packet is proposed in [16]. Consequently, the confidential (RoI) and the public (BG) packets can be sorted, from the highest to the lowest priority. Therefore, at each TS, the associated index ind in (2) can be set to 1, indicating that we choose the $L_p(L_s)$ most important packets to be sent during each TS.

B. Signaling Design for Semi-adaptive Image Transmission

After preparing fountain-coded packets c_l at the application layer based on (2), in this subsection, we elaborate on the design of transmit signal within a given frame at PHY. In order to safeguard data security of confidential packets, the transmit signal is combined with AN, while public BG packets are sent directly, using a beamforming vector $\mathbf{w}^\top \triangleq \hat{\mathbf{h}}_{sd}^\dagger / \|\hat{\mathbf{h}}_{sd}\|$. Hence, each fountain-coded packet has one of the following forms in the transmitting frame:

$$\begin{cases} \mathbf{x}_p = \sqrt{P_p} \mathbf{w} m_p, & \text{if } \Psi_0 \\ \mathbf{x}_s = \sqrt{\zeta P_s} \mathbf{w} m_s + \sqrt{\frac{(1-\zeta)P_s}{(n_T-1)}} \mathbf{G} \mathbf{v}_{AN}, & \text{if } \Psi_1 \end{cases} \quad (4)$$

where \mathbf{x}_p and \mathbf{x}_s correspond to the transmitted PHY signal of a public fountain-coded packet and a confidential one, respectively. Moreover, $m_k, \mathbf{v}_{AN} \in \mathbb{C}^{(n_T-1) \times 1}$, and P_k ($k \in \{s, p\}$) denote the unit-power information-bearing signal, i.e., the modulated version of the corresponding encoded packets, the AN with i.i.d. elements $v_i \sim \mathcal{CN}(0, 1)$, and the transmit power, respectively. We note that $0 < \zeta < 1$ shows the power allocation ratio between the information-bearing signal and the AN. We also note that the columns of $\mathbf{G} \in \mathbb{C}^{n_T \times (n_T-1)}$ and \mathbf{w} form an orthogonal basis. In other words, the source node \mathcal{S} adjusts its beamforming vector \mathbf{w} , based on the estimation of legitimate link $\hat{\mathbf{h}}_{sd}$, and injects AN to the original signal in a way that the legitimate link is not affected by the injected noise. Consequently, the received signal at \mathcal{D} when sending public and confidential data are expressed, respectively, as

$$\begin{aligned} y_D^p &= \sqrt{P_p} \rho r_D^{-\frac{\eta}{2}} \|\hat{\mathbf{h}}_{sd}\| m_p + \sqrt{(1-\rho^2)P_p} r_D^{-\frac{\eta}{2}} \mathbf{w}^\top \hat{\mathbf{e}}_{sd} m_p + n_D, \\ y_D^s &= \sqrt{\zeta P_s} \rho r_D^{-\frac{\eta}{2}} \|\hat{\mathbf{h}}_{sd}\| m_s + \sqrt{\zeta(1-\rho^2)P_s} r_D^{-\frac{\eta}{2}} \mathbf{w}^\top \hat{\mathbf{e}}_{sd} m_s + \sqrt{\frac{(1-\zeta)(1-\rho^2)P_s}{(n_T-1)}} r_D^{-\frac{\eta}{2}} \hat{\mathbf{e}}_{sd}^\top \mathbf{G} \mathbf{v}_{AN} + n_D. \end{aligned} \quad (5)$$

Based on (5), the instantaneous received signal-to-interference-plus-noise ratio (SINR) at \mathcal{D}^3 is formulated as

$$\gamma_D^s = \frac{\zeta \rho^2 P_s \|\hat{\mathbf{h}}_{sd}\|^2}{(1-\rho^2)P_s + r_D^\eta \sigma_n}, \quad \gamma_D^p = \frac{\rho^2 P_p \|\hat{\mathbf{h}}_{sd}\|^2}{(1-\rho^2)P_p + r_D^\eta \sigma_n}. \quad (6)$$

³Notably, the second term in (5) denotes the interfered AN at the legitimate link due to channel uncertainty.

Invoking the expression for γ_D^p in (6), at the beginning of public TSs, \mathcal{S} calculates the number L_p of public encoded-packets which should be prepared to construct the transmit frame as follows

$$L_p = \left\lceil \frac{BT}{b} \log_2(1 + \gamma_D^p) \right\rceil. \quad (7)$$

Obviously, (7) ensures that all L_p public packets can be successfully decoded by Bob without any error using capacity-achieving codes at PHY. Therefore, we can meet the delay requirements of packet-based image delivery via utilizing multi-packet transmission of public data. Similarly, for the transmission of confidential packets, we also opt for finding a suitable number L_s of transmit packets during each TS to satisfy the security constraints as well as addressing the delay limits. This is studied in the subsequent section.

In the case of transmitting confidential data, it is also of great importance to investigate the received signal $y_{E_i}^s$ and the instantaneous received SINR $\gamma_{E_i}^s$ at passive Eves for $i \in \Phi_E$. Hence, for the proposed scenario, we have

$$\begin{aligned} y_{E_i}^s &= \sqrt{\zeta P_s} \mathbf{w}^T \mathbf{h}_{se_i} m_s + \sqrt{\frac{(1-\zeta)P_s}{(n_T-1)}} \mathbf{h}_{se_i}^T \mathbf{G} \mathbf{v}_{AN} + n_{E_i}, \\ \gamma_{E_i}^s &= \frac{\zeta P_s r_i^{-\eta} |\mathbf{w}^T \mathbf{h}_{se_i}|^2}{(1-\zeta)P_s \|\mathbf{h}_{se_i}^T \mathbf{G}\|^2 r_i^{-\eta} / (n_T-1) + \sigma_n}, \end{aligned} \quad (8)$$

where \mathbf{h}_{se_i} denotes the fading channel from \mathcal{S} to the i -th Eve.

IV. PERFORMANCE ANALYSIS

A. Preliminaries

In this subsection, we first provide two useful lemmas which are used during our subsequent performance analysis.

Lemma 1. *Considering the NCE case for the randomly located Eves, where the equivalent SINR of the wiretap channel is expressed by $\gamma_E^{\text{NCE}} \triangleq \max_{i \in \Phi_E} \gamma_{E_i}^s$, the CDF of γ_E^{NCE} is expressed as*

$$F_{\gamma_E^{\text{NCE}}}(\omega) = \exp \left(-\beta \lambda_E \left(\zeta \frac{P_s}{\sigma_n} \right)^{\frac{2}{\eta}} \omega^{-\frac{2}{\eta}} \left(1 + \frac{1/\zeta - 1}{n_T - 1} \omega \right)^{1-n_T} \right), \quad (9)$$

where $\beta = \pi \Gamma(1 + \frac{2}{\eta})$, η , $\frac{P_s}{\sigma_n}$, and ζ denote the path-loss exponent, the transmit SNR of confidential packets, and the AN allocation ratio, respectively.

Proof. See Appendix A. ■

$$\mathcal{L}_{\gamma_E^{\text{CE}}}(s) = \exp\left(-2\pi\lambda_E\mathcal{B}\exp\left(\frac{\zeta s}{2}\right)(a_1 s)^{\frac{n_{\text{T}}-1+2/\eta}{2}}W_{\frac{1-n_{\text{T}}+2/\eta}{2}, \frac{2-n_{\text{T}}-2/\eta}{2}}(\zeta s)\right) \quad (11)$$

Lemma 2. *Considering the CE scenario for the randomly distributed Eves in our system model, where the instantaneous SINR of the equivalent wiretap channel is $\gamma_E^{\text{CE}} \triangleq \sum_{i \in \Phi_E} \gamma_{E_i}^s$, the CCDF of γ_E^{CE} is given by*

$$\overline{F}_{\gamma_E^{\text{CE}}}(\omega) \approx \sum_{k=0}^K \binom{K}{k} (-1)^k \mathcal{L}_{\gamma_E^{\text{CE}}}\left(\frac{k\varphi}{\omega}\right), \quad (10)$$

where K represents the number of terms used in the approximation⁴, $\varphi = \frac{K}{\sqrt{K!}}$, and $\mathcal{L}_{\gamma_E^{\text{CE}}}(s)$ exhibits the Laplace transform of the equivalent wiretap channel, which can be expressed as shown in (11) at the top of this page, with $\mathcal{B} = \frac{B(\frac{2}{\eta}, 1 - \frac{2}{\eta})}{\eta} \varrho^{\frac{1-n_{\text{T}}+2/\eta}{2}}$, $\varrho = (1 - \zeta) \frac{P_s}{\sigma_n} / (n_{\text{T}} - 1)$, $\zeta = \zeta(n_{\text{T}} - 1) / (1 - \zeta)$, and $a_1 = \zeta \frac{P_s}{\sigma_n}$.

Proof. See Appendices B and C. ■

B. QVP Derivation

To investigate the performance of our proposed packet-based delay-aware image transmission scheme, the quality-of-service violation probability (QVP) metric is examined. In comparison with the well-known secrecy outage probability (SOP) metric, QVP reflects a more comprehensive description regarding the system's performance in terms of the delay, the reliability, and the security level [18]. To be specific, SOP characterizes the probability with which the file is reliably received at \mathcal{D} , without any information leakage at Eves. In contrast, QVP calculates the probability with which the file is reliably received at legitimate destination within the given delay bound, without any information leakage at Eves. The QVP can be described as

$$\mathcal{P}_{\text{QVP}} = \Pr(T_D > D_{\text{lim}}) + \Pr(T_D \leq D_{\text{lim}}) \Pr(T_E \leq T_D), \quad (12)$$

where T_D denotes the number of TSs required by \mathcal{D} to completely recover the file, and T_E denotes the number of TSs required by the set of Eves to obtain all N_{roi} confidential packets in Π_s . Inspecting (12), one can infer that the first term reflects the delay violating probability, i.e.,

⁴It was shown in [25] that the provided approximation matches well with the corresponding exact expression for $K > 5$.

the probability with which the file cannot be successfully delivered from source to the legitimate destination within the tolerable delay D_{lim} . The second term in (12) shows the probability of the event that Eves obtain all N_{roi} confidential packets before the file delivery at destination is over, or the accumulation of their corresponding packets is accomplished simultaneously.⁵ For our proposed scheme, this is interpreted as the file intercept probability (FIP), which illustrates that the image delivery is not secured although the delay limit is met. In other words, Eves can obtain their information regarding the entire image as soon as all confidential (RoI-related) packets have been correctly received. Hence, T_E equals the number of TSs needed by Eve to correctly get N_{roi} RoI fountain packets. Summation of the two terms in (12) characterizes the probability with which the intended QoSec of our proposed scheme is violated.

Remark 2: Invoking (12), one can infer that by tending D_{lim} to infinity, the QVP simplifies to the special case of delay-insensitive systems. In this case, the QVP is dominated by the second term of (12), i.e., the FIP. This indicates that the designers should contribute to achieve superiority for the legitimate link against the wiretap channels to decrease the FIP. On the other hand, in a delay-sensitive systems with stringent delay requirements, i.e., small D_{lim} , the probability of \mathcal{P}_{QV} is dominated by the first term of (12). Remarkably, our proposed method considers both the packet accumulation enhancement at \mathcal{D} via utilizing multi-packet transmission (7), and the legitimate link improvement against Eves through injecting AN (5).

In the following, we derive a closed-form expression for the QVP metric. Toward this end, we note that the discrete RV T_D in (12) can be rewritten as

$$T_D = \bar{N}_{bg} + \frac{N_{roi}}{L_s} + N_D^{out}, \quad (13)$$

where \bar{N}_{bg} denotes the number of TSs required for delivering all N_{bg} public packets. Mathematically speaking, we have $\bar{N}_{bg} \triangleq |\mathcal{T}_p|$, where \mathcal{T}_p is the set of TSs used for delivering public data packets. By invoking (7) and the definition of \mathcal{T}_p , one can infer that \bar{N}_{bg} depends on the legitimate channel condition during file delivery. Moreover, although obtaining the exact expression for \bar{N}_{bg} is intractable, one can approximate \bar{N}_{bg} as follows

$$\bar{N}_{bg} \approx \left\lceil \frac{N_{bg}}{\sum_{k=0}^{+\infty} k p_{bg,k}} \right\rceil, \quad (14)$$

⁵We emphasize that in this article, in comparison with [15] and [16], we have assumed a more stringent condition on image recovery at Eves by considering the fact that recovering all RoI regions at Eves will suffice the image delivery to be intercepted completely. We also control the partial information leakage of RoI packets to Eves, which is addressed in the next subsection.

where the denominator denotes the expected number of fountain-coded public packets sent within a TS, and $p_{\text{bg},k}$ shows the probability with which k public packets are delivered to \mathcal{D} within a slot successfully. Thus, we have the following expression for $p_{\text{bg},k}$

$$p_{\text{bg},k} = \Pr\left(k \leq \frac{BT}{b} \log_2(1 + \gamma_D^p) < k + 1 \mid \Psi_0\right) \stackrel{(a)}{=} \left[\left(\gamma(n_\tau, \frac{\gamma_u}{\kappa_p}) - \gamma(n_\tau, \frac{\gamma_l}{\kappa_p}) \right) / \Gamma(n_\tau) \right] \frac{\mathbf{1}_{(\gamma_l < \gamma_u)}}{\Pr(\Psi_0)}, \quad (15)$$

where $\kappa_p = \frac{\rho^2 P_p}{(1-\rho^2)P_p + r_D^\eta \sigma_n}$, $\gamma_l = 2^{kb/(BT)} - 1$, $\gamma_u = \min\{\kappa_p \nu, 2^{(k+1)b/(BT)} - 1\}$, and ν denotes the decision threshold in (2). We note that (a) follows from [33, Eq. (3.382.5)]. Moreover, it is assumed that $\gamma_l < \gamma_u$, which is determined by the indicator function $\mathbf{1}_{(\gamma_l < \gamma_u)}$.

The second term in (13) denotes the required TSs for sending N_{roi} confidential packets. Finally, N_D^{out} shows the number of outage events for the legitimate link of \mathcal{S} -to- \mathcal{D} . By defining $\Upsilon(k, m; p) = \binom{k+m-1}{k} p^k (1-p)^m$, the following propositions facilitate the derivation of QVP.

Proposition 1. *The PMF of T_D can be expressed as*

$$f_{T_D}(k) = \Pr(T_D = k) = \Upsilon\left(k - \tilde{N}, \frac{N_{\text{roi}}}{L_s}; \Omega\right), k \geq \tilde{N}, \quad (16)$$

where $\tilde{N} \triangleq \bar{N}_{\text{bg}} + \frac{N_{\text{roi}}}{L_s}$, $\Omega = \frac{\mathbf{1}_{(\theta \geq \kappa_s \nu)}}{\Pr(\Psi_1)} \left(\gamma(n_\tau, \frac{\theta}{\kappa_s}) - \gamma(n_\tau, \nu) \right) / \Gamma(n_\tau)$, $\kappa_s = \frac{\rho^2 \zeta P_s}{(1-\rho^2)P_s + r_D^\eta \sigma_n}$, and $\theta = 2^{\frac{L_s b}{BT}} - 1$.

Proof. See Appendix D. ■

As a result, we can derive the expression for the first term of QVP in (12) as

$$\Pr(T_D > D_{\text{lim}}) = 1 - \sum_{k=\tilde{N}}^{D_{\text{lim}}} \Upsilon\left(k - \tilde{N}, \frac{N_{\text{roi}}}{L_s}; \Omega\right). \quad (17)$$

Proposition 2. *We have the following distribution for T_E*

$$\Pr(T_E \leq k) = \sum_{l=\frac{N_{\text{roi}}}{L_s}}^k \Upsilon\left(l - \frac{N_{\text{roi}}}{L_s}, \frac{N_{\text{roi}}}{L_s}; \Lambda_c\right), \quad (18)$$

where $c \in \{\text{NCE}, \text{CE}\}$ reflects which type (CE or NCE scenario) of eavesdropping strategy is run by Eves through the network, $\Lambda_{\text{NCE}} = \Pr(\Psi_1) \exp\left(-\beta \lambda_E (\zeta P_s / \theta)^{\frac{2}{\eta}} \left(1 + \frac{1/\zeta - 1}{n_\tau - 1} \theta\right)^{1-n_\tau}\right) + \Pr(\Psi_0)$, and $\Lambda_{\text{CE}} = \Pr(\Psi_1) \left[1 - \sum_{k=0}^K \binom{K}{k} (-1)^k \mathcal{L}_{\gamma_{\text{CE}}^E}\left(\frac{k\varphi}{\theta}\right)\right] + \Pr(\Psi_0)$.

Proof. See Appendix E. ■

Based on the provided discussions in this subsection, by invoking (12), one can rewrite the QVP metric as

$$\mathcal{P}_{QV} = \Pr(T_D > D_{lim}) + \sum_{k=\tilde{N}}^{D_{lim}} \Pr(T_D = k) \Pr(T_E \leq k). \quad (19)$$

Therefore, substituting (16), (17), and (18) into (19) completes the derivation of QVP for our proposed scheme.

C. Data Rate Adjustment to Assure Security for Confidential Packets

In our proposed scheme, to meet the delay constraints in a practical transmission scenario, the number of public packets that are called to be sent during each slot is carefully set owing to the multi-packet adaptive transmission of public packets (See Eq. (7)). The focus is now shifted toward the procedure of delivering confidential packets. With this regard, we aim to control the partial information leakage of confidential packets to Eves. Mathematically speaking, we ensure the intercept probability (IP) of sending confidential packets to be less than a desired threshold ϵ_{IP} . The IP metric describes the probability with which Eves intercept the transmitted confidential frame, given the transmission rate of source. Accordingly, by adjusting ϵ_{IP} , one can achieve a desired security level for the proposed scheme. Based on the aforementioned discussions, one can satisfy the following inequality

$$\mathcal{IP} \triangleq \Pr(\Psi_1) \Pr\left\{ \frac{BT}{b} \log_2(1 + \gamma_E^c) > L_s \mid \Psi_1 \right\} \leq \epsilon_{IP}. \quad (20)$$

where $c \in \{\text{NCE}, \text{CE}\}$. Then, (20) can be simplified to obtain an acceptable range for the number, L_s , of confidential packets that should be chosen to form confidential data frame. Hence, the following proposition is provided.

Proposition 3. *The acceptable range for the number L_s of packets comprising confidential data, based on limiting the transmission scheme to have an IP less than or equal to ϵ_{IP} is given by*

$$L_s \geq \frac{BT}{b} \log_2 \left(1 + F_{\gamma_E^c}^{-1} \left(1 - \frac{\epsilon_{IP}}{\Pr(\Psi_1)} \right) \right), \quad (21)$$

where $F_{\gamma_E^c}$ is derived in Lemma 1 and 2.

The proof of Proposition 3 can be obtained through a straightforward manipulation on the definition of IP in (20) and using the fact that the CDF $F_X(x)$ is a monotonically increasing

function on x .

V. OPTIMIZED LEARNING-BASED IMAGE TRANSMISSION

In this section, we aim to optimize the network parameters to enhance the overall system performance. By invoking (16)–(19), one can infer that the QVP is affected by different channel conditions, as well as the image size and the location of the legitimate node being serviced. More specifically, every time a new image is scheduled to be transmitted to the legitimate receiver \mathcal{D} , or when a new device is authenticated to receive packets from \mathcal{S} , the source should adjust its transmission parameters, including the power allocation ratio ζ between information and AN, the transmission power for public and confidential packets, denoted by P_p and P_s , respectively, and the decision threshold ν on whether to send public or confidential packets. The transmission rate $R_s = L_s b$ of confidential packets can be optimized as well. Moreover, the transmitter should be robust against different states of channel imperfection, which is modeled by parameter ρ in this paper.

Mathematically speaking, for each complete round of image delivery from \mathcal{S} to a legitimate receiver, the optimal transmission parameters $(\zeta^*, P_p^*, P_s^*, \nu^*)$ to minimize the QVP metric can be found from the following optimization problem

$$\begin{aligned} & \underset{\zeta, P_p, P_s, \nu, L_s}{\text{minimize}} && \mathcal{P}_{QV} \\ & \text{s.t.} && \mathcal{IP} \leq \epsilon_{\text{IP}}, \quad 0 < \zeta \leq 1, \quad \nu > 0, \quad \gamma_{\min} < \frac{P_s}{\sigma_n}, \frac{P_p}{\sigma_n} \leq \gamma_{\max}, \quad L_s | N_{\text{roi}}, \end{aligned} \quad (22)$$

where γ_{\min} and γ_{\max} represent the minimum and the maximum available transmit SNR at the source node \mathcal{S} . In addition, the last constraint indicates that L_s is a divisor of N_{roi} .

The proposed optimization problem is a mixed-integer non-linear programming (MINLP) due to its non-linear (and highly non-convex) objective and constraints. Therefore, obtaining an analytic expression for the optimal transmission parameters $(\zeta^*, P_p^*, P_s^*, \nu^*, L_s^*)$ is intractable. Traditionally, (22) could be solved via numerical algorithms leading to a large computational complexity. In contrary, we propose a learning-based scheme to solve (22) in an efficient way.

We now elaborate on our learning-based scheme to effectively attain optimal transmission parameters. In our proposed scheme, \mathcal{S} utilizes a deep neural network (DNN) to learn the non-trivial mapping from the system's configurations, i.e., input image size, including the confidential

and public packets, the location of the legitimate receiver, and the channel statistics to the optimal transmission parameters that minimizes the QVP. This mapping can be formulated as

$$(\zeta^*, P_p^*, P_s^*, \nu^*, L_s^*) = \mathcal{F}(N_{\text{roi}}, N_{\text{bg}}, r_D, \rho). \quad (23)$$

In the following, we propose our DNN's architecture for solving (23), which is composed of fully-connected layers in a feedforward network. It is worth mentioning that the DNNs, specifically the feedforward neural networks, have shown to be capable of performing very complex tasks and obtain an input-output map that approximates any measurable function [27]. Therefore, utilizing DNNs is an efficient strategy to solve the problem in (22).

A. Network Architecture

We first provide a brief overview of feedforward DNNs. A general architecture for a feedforward neural network with fully-connected layers is composed of an input layer, an output layer, and K hidden layers. The output of each layer is the input of its sequential layer. The k -th layer, $k = 1, \dots, K + 1$, has u_k neurons, and the $u_k \times 1$ output vector of the k -th layer ($2 \leq k \leq K + 2$) can be written as

$$\mathbf{x}_k = f_k(\mathbf{W}_k \mathbf{x}_{k-1} + \mathbf{b}_k), \quad (24)$$

where f_k is the activation function of layer k , \mathbf{W}_k and \mathbf{b}_k respectively denote the weight matrix and the bias vector of the k -th layer. Notably, \mathbf{x}_0 is the input vector to the DNN. According to (24), each neuron is responsible for computing quite lightweight operations. The combination of multiple neurons through stacked fully-connected layers, the proposed DNN can obtain an overall input-output mapping to emulate desired functions [28, Theorem 1]. We can now elaborate on our proposed DNN for the content-aware wireless image transmission scheme. The problem is to fine-tune the weights and biases of (24) to efficiently estimate (23).

Considering an E2E realization of image delivery from the source node, \mathcal{S} , to a legitimate destination \mathcal{D} , we utilize a feedforward DNN, in which the following information are fed into the network as input: The number of confidential and public source packets; the level of wireless channel imperfection estimated at \mathcal{S} , which was modeled via the parameter ρ in (1); and, the location of the legitimate destination \mathcal{D} . We opt for producing vector $\mathbf{x}_{K+2} = [\zeta^*, P_p^*, P_s^*, \nu^*, L_s^*]^T$ corresponding to the optimal transmission parameters at the output layer. As illustrated in Fig.

2, between the input and output layers, $K = 4$ dense layers are deployed each of which contain a fully-connected layer followed by a batch normalization (BN) block. Notably, the BN is performed with the aim of enhancing the generalization properties of our DNN, and making the learning process more stable. The BN block performs $\hat{x}_{k,i} = \frac{x_{k,i} - \mu_B}{\sqrt{\sigma_B^2 + \epsilon}}$, $y_{k,i} = \lambda_i \hat{x}_{k,i} + \delta_i$, on its input \mathbf{x}_k , $k \in \{2, \dots, K+1\}$ for all \mathbf{x}_k 's in a mini-batch, where $x_{k,i}$, $i \in \{1, \dots, u_k\}$ is the i -th input of BN block at the k -th layer, $y_{k,i}$ is the corresponding i -th output of the BN block, λ_i and δ_i are learnable parameters along with the other network parameters. Moreover, μ_B and σ_B^2 are the mean and variance of training data over a mini-batch of size m , while ϵ is for the sake of stability. Activation functions of hidden neurons in our proposed DNN are chosen to be rectified linear unit (ReLU), which is defined as $f_k^{\text{ReLU}}(x) \triangleq \max(0, x)$, $2 \leq k \leq K+1$. The output layer is obtained from a fully-connected layer followed by a linear activation function.

B. Training of the Proposed DNN: Train Offline, Use Online

In order to find an appropriate estimation for (23), the weights and biases in (24) need to be adjusted. Accordingly, the weights $\mathbf{W} = [\mathbf{W}_2, \dots, \mathbf{W}_{K+2}]$ and the biases $\mathbf{B} = [\mathbf{b}_2, \dots, \mathbf{b}_{K+2}]$ as well as the scale and shift parameters of BN blocks in hidden layers, denoted respectively by $\mathbf{\Lambda} = [\boldsymbol{\lambda}_2, \dots, \boldsymbol{\lambda}_{K+1}]$ and $\mathbf{\Delta} = [\boldsymbol{\delta}_2, \dots, \boldsymbol{\delta}_{K+1}]$, are configured. This adjustment is carried out in a supervised manner via training our DNN with a training set $\mathcal{T} = \{(\mathbf{r}_n, \mathbf{p}_n^*)\}$, $n = 1, \dots, N_{\mathcal{T}}$, with $N_{\mathcal{T}} = |\mathcal{T}|$ training tuples, where $\mathbf{p}_n^* = [\zeta^*, P_p^*, P_s^*, \nu^*, L_s^*]^T$ is the vector of desired transmission parameters corresponding to a realization of system with configuration parameters $\mathbf{r}_n = [N_{\text{roi}}, N_{\text{bg}}, r_D, \rho]^T$. Note that the training set can be obtained via prevalent numerical methods for solving an optimization problem through an offline phase [8], [29]. Using the examples provided in \mathcal{T} , the DNN gradually learns to predict the transmission parameters for new realizations of \mathbf{r}_n as well. Mathematically speaking, the training process opt for adjusting the weights and biases of our DNN with the goal of minimizing the loss between actual and desired output vector, which is formulated as follows

$$\underset{\mathbf{W}, \mathbf{B}, \mathbf{\Lambda}, \mathbf{\Delta}}{\text{minimize}} \quad \frac{1}{N_{\mathcal{T}}} \sum_{n=1}^{N_{\mathcal{T}}} \ell \left(\mathbf{x}_{K+2}^{(n)}(\mathbf{W}, \mathbf{B}, \mathbf{\Lambda}, \mathbf{\Delta}), \mathbf{p}_n^* \right), \quad (25)$$

where $\mathbf{x}_{K+2}^{(n)}(\mathbf{W}, \mathbf{B}, \mathbf{\Lambda}, \mathbf{\Delta})$ denotes the output of DNN corresponding to the n -th training input, \mathbf{p}_n^* is the desired output, and $\ell(\cdot, \cdot)$ is any desired error measure between these two. We employ mean-squared-error (MSE) $\|\mathbf{x}_{K+2}^{(n)}(\mathbf{W}, \mathbf{B}, \mathbf{\Lambda}, \mathbf{\Delta}) - \mathbf{p}_n^*\|^2$ as a widely-used error measure in this

paper. The minimization of (25) can be handled by off-the-shelf gradient descent-based methods specifically developed for training DNNs [27], which is not reviewed here.⁶

After that the training phase is completed, i.e, the minimization problem of (25) converges to a relatively low MSE, our DNN achieves an acceptable approximation for the mapping in (23). Afterward, when a new configuration, \mathbf{r}^{new} , is defined for the system, i.e., a new image is scheduled to be sent or a new legitimate node is signed in to the network, the corresponding transmission parameters can be obtained without the need to solve (22) again. Instead, it suffices to compute the output of the trained DNN, using a forward propagation with the new input \mathbf{r}^{new} in a real-time manner.

Remark 3: Compared with the conventional approaches which mandate the system to perform iterative methods from scratch—which actually imposes much delay on practical systems—every time one or more configurations are altered (e.g., the source should send an image), our proposed procedure brings about a significant decrease in computational complexities during the online phase of using the trained DNN. This is actually in line with the requirements of our practical delay-aware model. More details are addressed in the following subsection.

C. Computational Complexity

Based on the provided discussions in Section V-B, we first stress that once the weights and biases in (25) are determined, the input-output relationship of the DNN can be calculated as the composition of affine combinations and activation functions of the neurons as proposed in (24). In other words, the main advantage of our proposed learning-based method is that one can perform most of the computations required for solving (22) offline, and only a few operations need to be calculated when the system configurations vary.

1) *Online phase:* When the trained DNN is exploited for predicting new outputs, it is required to compute the output of each neuron in the DNN, moving forward from the input layer to the output layer. Therefore, by invoking (24) and the BN adjustment formula, one can argue that $\sum_{k=2}^{K+2} u_{k-1}u_k + \sum_{k=2}^{K+1} u_k$ real multiplications, together with calculating $\sum_{k=2}^{K+2} u_k$ scalar activation functions f_k are incurred during online computation.⁷ Notably, the activation functions are elementary functions which do not impose any significant computational complexities to the

⁶We have chosen the widely-adopted adaptive moment estimation (Adam) optimizer algorithm for minimizing (25) [30]. The convergence of our training process is validated in the simulation results.

⁷The incurred complexity of additions is neglected compared with the complexity of multiplications.

network. Consequently, finding the output of our trained DNN for a given realization vector comprises negligible complexity as it simply requires the calculation of forward propagation through the trained DNN.

2) *Offline phase*: The offline phase, as proposed in Section V-B, includes training set generation and its utilization to train the network. The training procedure can be carried out efficiently, using off-the-shelf stochastic gradient descent algorithms with fast convergence [27]. Generating the training set \mathcal{T} requires the proposed problem in (22) to be solved $|\mathcal{T}|$ times for different realizations of the system parameters.⁸ Although it seems to be in contradiction with the purpose of using DNNS, but this is not the case for the following reasons:

- (i) The training phase—including the data set generation and DNN adjustment—is performed *offline*. In this manner, a much higher computational time and complexity can be afforded with significantly less constraints than a real-time computation [29].
- (ii) The update procedure of training set is done sporadically. In other words, generating training samples can be done with a *much greater time-scale* than the real-time configuration settings.

VI. NUMERICAL RESULTS AND DISCUSSIONS

In this section, we present several numerical examples to verify our derived closed-form expression for the QVP metric. Moreover, some relevant benchmarks are compared with our proposed scheme to show the efficiency of our hybrid transmission scheme. The impact of multiple randomly-located Eves on the performance of our proposed scheme together with some insights on design parameters are also provided. The convergence of our ML-based optimization problem is validated by investigating the training performance of our proposed DNN. Numerical results show the effectiveness of utilizing DNN for employing optimal transmission parameters. The codes are implemented in MATLAB, and were run on a 64-bit 1.80 GHz Intel(R) Core(TM) i7-8550U CPU. Moreover, the offline phase of data set generation and DNN training were run on Intel(R) Xeon(R) Silver 4114 CPU running at 2.20 GHz. In order to accelerate the offline computations, the workflow was scaled up by leveraging a parallel pool of multiple distributed workers [34].

For the following experiments, similar to [16] and [17], we consider the nodes to be located on a normalized two-dimensional region, where \mathcal{S} is placed at the origin without loss of generality.

⁸We use the genetic algorithm [31] for numerically solving (22) and obtaining an experimental training set \mathcal{T} . This is elaborated in the next section.

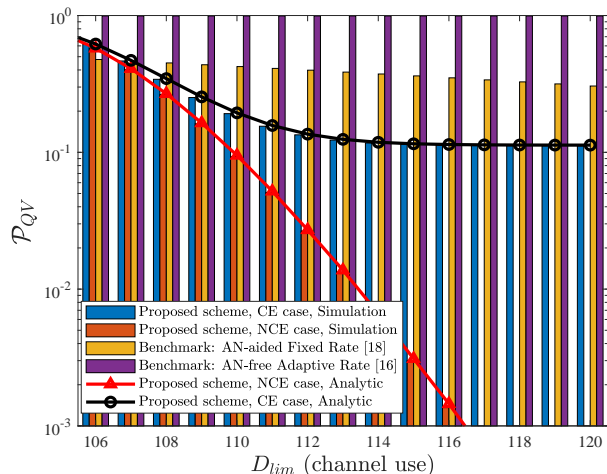


Fig. 3: QVP versus D_{lim} for our proposed scheme.

The passive Eves are assumed to be distributed according to homogeneous PPP Φ_E with density $\lambda_E = 0.2$ (except for Fig. 5 in which we sweep the value of λ_E to see its effect on system performance). We set the path loss exponent to $\eta = 4$, and $\frac{BT}{b} = \frac{50}{8}$ during the simulations [16]. For the following figures, the source node is assumed to be equipped with $n_T = 8$ transmit antennas, except for Fig. 4 in which we examine the effect of n_T . For Figs. 3–5, we consider the legitimate receiver \mathcal{D} to be located at $[2, -2]$. We also suppose $N_{roi} = 300$ and $N_{bg} = 200$ confidential and public packets, respectively, are scheduled to be delivered with the transmit SNR of 30 dB, while the allocation ratio between the information signal and the AN is considered $\zeta = 0.5$. The fixed rate of sending confidential packets is also set to $L_s = 20$ for the first three simulation figures. We stress that the optimal transmission parameters, including the optimal transmit SNRs together with the power allocation ratio, and the optimal confidential transmission rate are evaluated and examined in the subsequent Figs. 6–9.

Fig. 3 illustrates the QVP versus the tolerable delay limit D_{lim} for our proposed scheme and two benchmarks. For this figure, the decision level ν is set to 6, and the channel correlation coefficient is set to $\rho = 0.95$ [25]. A security level of $\epsilon_{IP} = 0.1$ is also imposed on the transmission of confidential packets based on (20). According to the figure, one can easily verify that for all values of D_{lim} , the experimental results match well with the analytical closed-form expressions obtained for the QVP in (19). The numerical results of this figure are obtained using Monte Carlo simulation over 10^5 realizations. Based on Fig. 3, it is clear that \mathcal{P}_{QV} starts to decrease with the increase in D_{lim} . Generally speaking, by relaxing the delay limit it becomes easier for the legitimate destination node to accumulate $N = N_{roi} + N_{bg}$ coded packets within the delay bound.

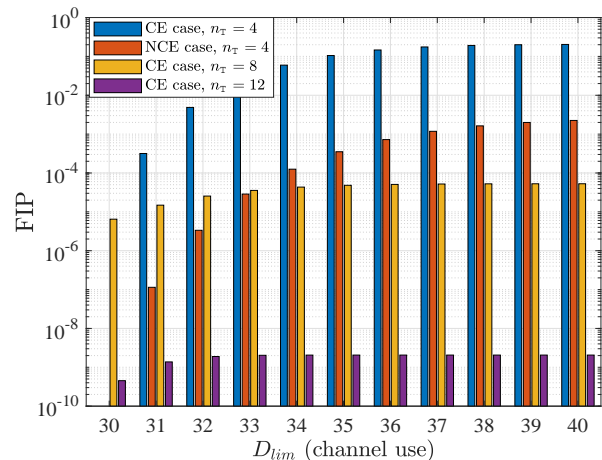


Fig. 4: The file intercept probability vs. D_{lim} for different values of n_T .

More specifically, for smaller values of D_{lim} , the QVP is reduced with the increase in D_{lim} . This is because, in this case, the QVP is directly dominated by the delay violating probability as discussed in Remark 2. However, in further increments of D_{lim} , \mathcal{P}_{QV} is also affected by the presence of totally passive Eves trying to improve their FIP. Therefore, the QVP might become saturated. This fact can be explicitly seen from Fig. 3, where for the CE strategy, in which the equivalent wiretap channel is the accumulation of all individual eavesdropping channels, the saturation occurs at moderate values of D_{lim} . However, for the NCE case, in which the eavesdroppers do not collude with each other, the monotonic decrease in QVP can be seen in the range of $106 < D_{lim} < 120$. This can be deduced from equations (18) and (19), together with Lemmas 1 and 2. Fig. 3 also demonstrates the outperformance of our hybrid approach for image delivery in comparison with two benchmarks: 1) The adaptive rate transmission with no AN injection (ARNAN) [16]; and, 2) The fixed-rate (multi-packet) AN-aided (FRANA) transmission [18]⁹. We can observe from the figure that the ARNAN case cannot achieve small values of QVP within the given range of delay limits in this figure, which means the utilization of adaptive multi-packet transmission is not solely sufficient to conquer wiretappers. This highlights the importance of AN injection in a wireless transmission environment comprising of multiple passive Eves. In contrast, the QVP of FRANA benchmark starts to decrease with a relatively small slope as the delay limit increases. In other words, with the increase in D_{lim} , where the existence of multiple Eves starts to affect the system's performance, the injected AN can help achieve smaller values of \mathcal{P}_{QV} . However, due to the fact that an adaptive transmission is not considered for this benchmark, the packet accumulation at \mathcal{D} is not properly addressed. On the contrary, our proposed scheme addresses both the packet accumulation at \mathcal{D} , via employing (7), and the AN injection for the confidential packets leading to a much lower \mathcal{P}_{QV} .

To investigate the secrecy of our proposed wireless image delivery, Fig. 4 demonstrates the FIP metric for different values of n_T . For this figure, we have $\epsilon_{IP} = 0.1$ and $\rho = 0.95$. Notably, we can see from the figure that our proposed scheme can achieve arbitrary small values of FIP, indicating the secrecy of our approach. Moreover, by increasing the number of transmit antennas deployed at \mathcal{S} , lower FIPs are achievable, owing to the establishment of beamforming vectors with pencil-sharp beams which further degrades the wiretap channels according to (8).

⁹We note that the authors in [18] actually considered only one packet per TS in their AN injection scheme. However, for the sake of fair comparison and without loss of generality, we consider a fixed number of packets to be transmitted in benchmark 2.

This figure also validates the discussions provided in Lemma 2 regarding the saturation of FIP by tending D_{lim} to infinity. Therefore, one can control the FIP to a certain limit by carefully designing the transmission parameters, even though a considerable time is allowed for Eves to intercept the file.

Fig. 5 shows \mathcal{P}_{QV} versus the density of distributed Eves considering the security level $\epsilon_{IP} = 0.01$ for confidential packets. Different values of channel imperfection are considered in this figure, where better performance can be achieved by having more accurate estimates about the legitimate link. We can see from the figure that the population density of Eves can highly affect the performance of the system when Eves are running in colluding mode. Accordingly, increasing λ_E can result in tending the QVP to 1 in CE case. This is because, for the CE scenario, the equivalent wiretap channel cumulatively depends on all individual eavesdropping channels, i.e., $\gamma_E^{CE} \triangleq \sum_{i \in \Phi_E} \gamma_{E_i}^s$. Thus, increasing λ_E , which likely increases the expected number of passive Eves, directly leads to the increase in FIP; thus the QVP. On the other hand, increasing λ_E does not directly affect the QVP in NCE case because the equivalent wiretap channel depends only on the strongest eavesdropping link. The slight increase of QVP in the NCE case is due to the fact that increasing λ_E will increase the probability of having an Eve with a high-quality link. Thus, the saturated QVP of the NCE case can be viewed as a reference range of QVP achievable for the proposed scheme.

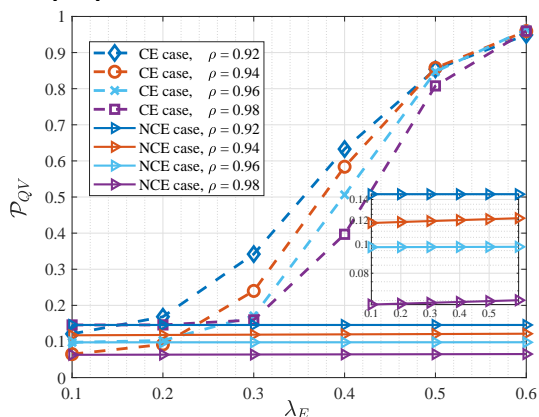


Fig. 5: The QVP vs. density of distributed Eves λ_E for different values of ρ

Learning Parameters	Values
Mini-batch size (m)	50
Maximum number of training epochs	500
Initial learning rate	0.001
Learning rate drop factor	0.9
Number of training samples ($ \mathcal{T} $)	3500
Number of validation samples	750
Number of neurons in the hidden layers	(32,16,16,8)
Optimizer	Adam [30]

TABLE I: Parameters for Training the Proposed DNN

Performance of the Proposed DNN:

In what follows, we investigate the training process of our proposed DNN. Moreover, the optimized performance of our learning-based scheme is also investigated. For the subsequent numerical experiments, we set $D_{lim} = 30$, $\epsilon_{IP} = 0.2$, $\gamma_{min} = 10$ dB, and $\gamma_{max} = 30$ dB. The

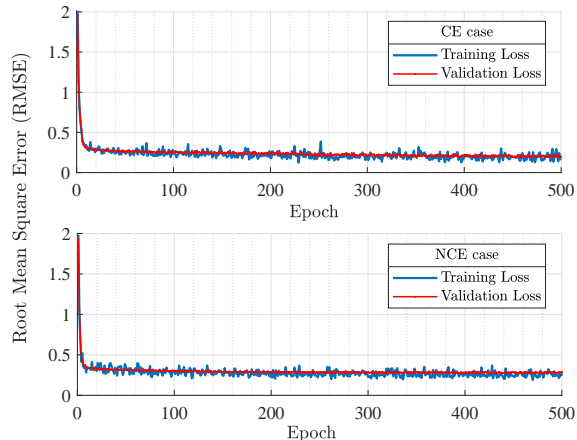


Fig. 6: Training and validation loss of the proposed DNN.

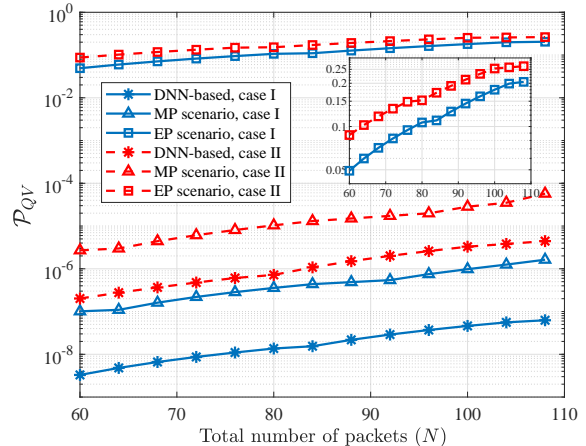


Fig. 7: QVP vs. the total number of packets for the NCE scenario with $\rho = 0.9$.

learning parameters used during the training process are summarized in Table I. A dataset of size 5000 is generated using the genetic algorithm [31] for solving (22) for the general parameters of $n_T = 8$, $\lambda_E = 0.2$, $D_{lim} = 30$. The learning process is facilitated via normalizing the transmit SNRs. More specifically, we have considered the change of variable $\tilde{P}_k^* \sigma_n \gamma_{max} = P_k^*$, for $k = \{s, p\}$. Similar reformulation is done for L_s^* by performing $N_{roi} \tilde{L}_s^* = L_s^*$ to lie in the interval $[0, 1]$.

Fig. 6 exhibits the training performance of our proposed DNN by investigating the average training and validation losses over epochs. Notably, we used a validation set during training to verify the generalization performance of our DNN.¹⁰ One can easily observe that the minimization problem (25) corresponding to the training process quickly converges to a small value. Interestingly, both losses do not increase over epochs which means, the employed training process is not confronted with overfitting/underfitting phenomena.

Figs. 7 and 8 illustrate the QVP versus the total number of packets, $N = N_{roi} + N_{bg}$, for two eavesdropping scenarios, i.e., NCE and CE, respectively. In these figures, two different locations are considered for the legitimate destination, which are shown by case I and case II in the figures. In Fig. 7, cases I and II correspond, respectively, to the case of \mathcal{D} being at $[1.8, -0.8]$ and $[2, -1]$. In Fig. 8, \mathcal{D} is located at $[2.4, 1.4]$ and $[2.6, 1.6]$ for cases I and II, respectively. In figures 7 and 8, the resultant QVP from our proposed DNN is compared with two related

¹⁰Due to the fact that during the training process some information about the validation set leaks to the DNN, we also had another set, i.e., the test set, for the final testing of the DNN. The validation and test sets are generated independently in the same manner as for the training set.

baselines. 1) The maximum power (MP) transmission scenario, in which the transmit SNR of source, for both types of confidential and public transmission, is set to its maximum level γ_{\max} ; and, 2) the equal power (EP) allocation between AN and information signal, in which we set $\zeta = 0.5$, while the remainder of the transmission parameters are set to their optimum values obtained from our DNN. The performance gain of our learning-based approach compared with the mentioned baselines can be clearly observed from the figures. To be more specific, our proposed learning-based approach has come up with an intelligent and flexible procedure to take optimal transmission parameters according to different system configurations. This was discussed in details in Section V. On the contrary, adopting MP or EP policies cannot provide the optimum QVP since they blindly choose the transmission parameters. For instance, according to the MP scenario, one can conclude that sending an image with maximum available power does not necessarily yield to the minimum achievable QVP. Instead, we should take the image content and the general configurations of the wireless system into account to choose the best option for the transmit power. As demonstrated by Figs. 7 and 8, the QVP of EP scenario is higher than our proposed scheme and the MP scenario. This observation highlights the importance of fine-tuning the AN signal based on different configurations [7]. It can be inferred from these figures that if the power allocation ration ζ between the AN and information signal is not properly adjusted, the resultant QVP tends to large values although maintaining optimal transmit powers. The rationale behind this effect is that the value one chooses for ζ not only determines the amount of AN employed for confusing Eves, but also affects the remaining power budget for transmitting the information signal. Finally, we can see that when the destination moves towards \mathcal{S} , better QVPs can be achieved which is in accordance with one's intuition.

Fig. 9 demonstrates our learning-based optimized QVP (\mathcal{P}_{QV}^*) versus the correlation coefficient between the legitimate channel, \mathbf{h}_{sd} , and the estimated one, $\hat{\mathbf{h}}_{sd}$, for different values of N_{bg} . In this figure, we consider the destination to be located at $[1.5, 1.5]$ and $[3, 3]$ for the CE and NCE scenarios, respectively. From the figure, one can see the effect of imperfect channel estimation on the overall performance of the system. Accordingly, by having accurate estimations of the legitimate channel, i.e., higher values of ρ , better system performance is achieved in terms of the QVP. Mathematically speaking, the higher the quality of the channel estimation is, the higher received SINR is obtained at \mathcal{D} , which can be easily verified from (6). The reason is twofold. First, with the increase in ρ , more accurate beamforming vector \mathbf{w} for transmitting the information-bearing signal can be designed at PHY based on (4). Hence, larger SINRs

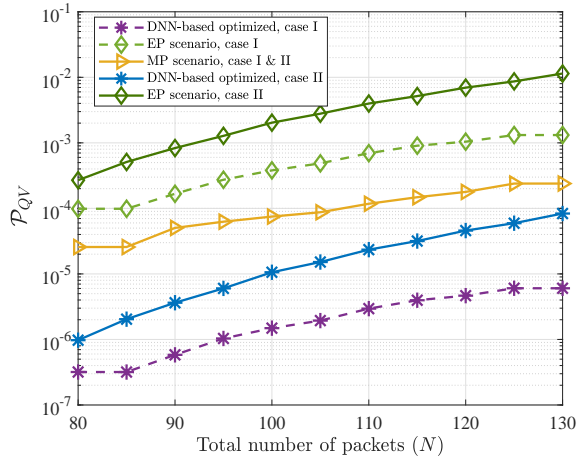


Fig. 8: QVP vs. the total number of packets for the CE scenario with $\rho = 0.75$.

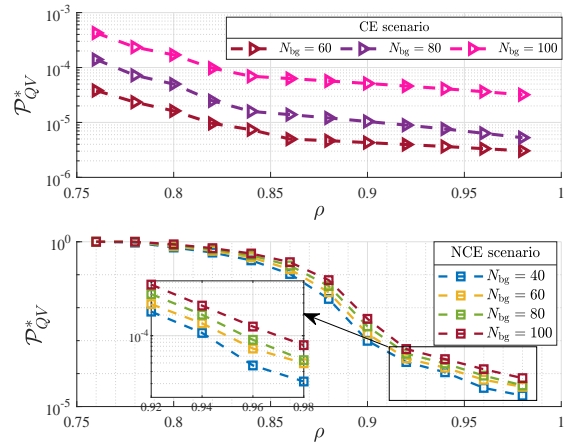


Fig. 9: Optimized QVP versus the channel correlation coefficient ρ .

are obtained at \mathcal{D} ; second, when the available estimation of the legitimate link becomes more accurate, the amount of AN signal which unwantedly exists in the legitimate link due to the imperfect design of the AN beamforming, $\mathbf{G}\mathbf{v}_{\text{AN}}$, decreases. This can be inferred from (4) and (5). We also emphasize that having greater values for the SINR at destination also results in higher rates for packet transmission according to (7). With a similar discussion on the derived formulas, having poor estimations of the legitimate channel may result in QVPs which might not be desirably small. In Fig. 9, we also examine the optimized QVP for different values of N_{bg} . Accordingly, increasing the number of N_{bg} will require more TSs to complete the file delivery which increases \mathcal{P}_{QV}^* for a fixed D_{lim} . This can also be verified from (13), (14), and (19). We note that according to this figure, one can see that a slight improvement in the quality of channel estimation leads to the fact that more packets can be sent within a given delay limit, while having the same QVP. For instance, if we set $\mathcal{P}_{QV}^* = 10^{-4}$, about 8% increase in ρ results in 25% increase in the number of packets allowed to be sent within the delay limit $D_{\text{lim}} = 30$ for the CE case. Similarly, for the NCE case, by 3% improvement in ρ , 1.5 times more packets can be transmitted.

VII. CONCLUSIONS

In this paper, a learning-assisted content-aware image transmission scheme is investigated, over a MISO channel in the presence of randomly distributed passive eavesdroppers. We consider the fact that not all regions of an image have the same priority from the security perspective. Thus, a hybrid multi-packet transmission scheme is proposed to assure security while taking

into account the delay limits of a practical image transmission scheme. To further reinforce the system's security, the source packets are encoded by an FC-based method at the application layer. A closed-form expressions for the QVP metric is derived to characterize the delay-aware performance of our proposed scheme. Moreover, we take advantage of a fully-connected DNN to minimize the QVP by maintaining optimized transmission parameters. Simulation results illustrate that our proposed learning-assisted scheme outperforms the state-of-the-art benchmarks by achieving considerable gains in terms of security and delay.

APPENDIX A

We first define $u = |\mathbf{w}^\top \mathbf{h}_{se_i}|^2$ and $v = \|\mathbf{h}_{se_i}^\top \mathbf{G}\|^2$. Notably, we have $u \sim \text{Exp}(1)$, and $v \sim \mathcal{G}(n_\tau - 1, 1)$. In addition, u and v are independent of each other, since \mathbf{w} and \mathbf{G} are orthogonal. Invoking (8) and by defining $\xi \triangleq \frac{1/\zeta - 1}{n_\tau - 1}$, we first derive the CDF $F_{\gamma_{E_i}}(\omega)$ of γ_{E_i} which can be expressed as

$$\begin{aligned} F_{\gamma_{E_i}}(\omega) &= \Pr\left(u < \frac{\xi \zeta P_s v + r_i^\eta \sigma_n}{\zeta P_s} \omega\right) = 1 - \mathbb{E}_v \left[e^{-\xi v \omega} e^{-\frac{r_i^\eta \omega}{\zeta P_s / \sigma_n}} \right] \\ &\stackrel{(a)}{=} 1 - \exp\left(-\frac{r_i^\eta \omega}{\zeta P_s / \sigma_n}\right) (1 + \xi \omega)^{1-n_\tau}, \end{aligned} \quad (26)$$

where (a) follows from [33, Eq. (3.326.1)]. Consequently, $F_{\gamma_E^{NCE}}(\omega)$ is formulated as follows

$$F_{\gamma_E^{NCE}}(\omega) = \mathbb{E}_{\Phi_E} \left[\prod_{i \in \Phi_E} \Pr(\gamma_{E_i} < \omega) \right] \stackrel{(b)}{=} \exp\left(\frac{-2\pi \lambda_E}{(1 + \xi \omega)^{n_\tau - 1}} \int_0^\infty r e^{\frac{-r^\eta \omega}{\zeta P_s / \sigma_n}} dr\right), \quad (27)$$

where (b) holds for the probability generating functional lemma (PGFL) over PPP [24]. Finally, calculating (27) with formula [33, Eq. (3.326.2)] completes the proof.

APPENDIX B

For the CE case, we first derive the Laplace transform of γ_E as follows

$$\begin{aligned} \mathcal{L}_{\gamma_E^{CE}}(s) &= \mathbb{E}_{\Phi_E, u, v} \left[e^{-s \sum_{i \in \Phi_E} \gamma_{E_i}^s} \right] \stackrel{(a)}{=} \mathbb{E}_{\Phi_E} \left[\prod_{i \in \Phi_E} \mathbb{E}_{u, v} \left[e^{-s \gamma_{E_i}^s} \right] \right] \\ &\stackrel{(b)}{=} \exp\left(-2\pi \lambda_E \underbrace{\mathbb{E}_{u, v} \left[\int_0^\infty r_i (1 - \exp(-s \gamma_{E_i}^s)) dr_i \right]}_{\mathcal{I}}\right), \end{aligned} \quad (28)$$

where (a) follows from the fact that γ_{E_i} 's, $i \in \Phi_E$ are independent of each other over u and v . In addition, (b) holds for the PGFL over PPP. According to (8), we can rewrite $\gamma_{E_i}^s = \frac{a_1 u}{a_2 v + r_i^\eta}$, with $a_1 = \zeta \frac{P_s}{\sigma_n}$ and $a_2 = (1 - \zeta) \frac{P_s}{\sigma_n} / (n_T - 1)$. Consequently, we proceed to solve the expected-valued integral term in (28). Hence, we have

$$\begin{aligned} \mathcal{I} &\stackrel{(c)}{=} \int_0^\infty r_i \mathbb{E}_v \left[\frac{a_1 s}{a_1 s + a_2 v + r_i^\eta} \right] dr_i \stackrel{(d)}{=} B \left(\frac{2}{\eta}, 1 - \frac{2}{\eta} \right) \frac{a_1 s}{\eta} \int_0^\infty (a_1 s + a_2 v)^{2/\eta-1} f_v(v) dv \\ &\stackrel{(e)}{=} \mathcal{B} e^{\frac{sa_1}{2a_2}} (a_1 s)^{\frac{n_T-1+2/\eta}{2}} W_{\frac{1-n_T+2/\eta}{2}, \frac{2-n_T-2/\eta}{2}} \left(\frac{a_1 s}{a_2} \right) \end{aligned} \quad (29)$$

where (c) follows from the fact that u and v are independent, (d) results from the transformation $r_i^\eta = y$ and using [33, Eq. (3.194.3)], and (e) follows by changing the variable $a_1 s + a_2 v = z$ and then using [33, Eq. (3.383.4)]. Moreover, $f_v(v) = \frac{v^{n_T-2} e^{-v}}{\Gamma(n_T-1)}$ and $\mathcal{B} = \frac{B(\frac{2}{\eta}, 1-\frac{2}{\eta})}{\eta} (a_2)^{\frac{1-n_T+2/\eta}{2}}$.

APPENDIX C

After deriving $\mathcal{L}_{\gamma_{E}^{\text{CE}}}(s)$, the CDF of γ_{E}^{CE} can be derived via utilizing inverse Laplace transform. However, this method requires considerable computation complexity, hence is almost intractable. Therefore, we utilize the following steps to provide an approximation of $\bar{F}_{\gamma_{E}^{\text{CE}}}(\omega)$ by introducing an intermediate RV denoted by \mathfrak{J} which obeys normalized Gamma distribution with parameter K . Therefore, we have

$$\bar{F}_{\gamma_{E}^{\text{CE}}}(\omega) = \mathbb{E}_{\Phi_E} \left[\Pr(\gamma_{E}^{\text{CE}} > \omega) \right] \stackrel{(a)}{=} \mathbb{E}_{\Phi_E} \left[\Pr \left(\frac{\gamma_{E}^{\text{CE}}}{\omega} > \mathfrak{J} \right) \right] \stackrel{(b)}{\approx} \mathbb{E}_{\Phi_E} \left[\left(1 - \exp \left(-\varphi \frac{\gamma_{E}^{\text{CE}}}{\omega} \right) \right)^K \right], \quad (30)$$

where (a) holds due to the fact that a normalized Gamma RV converges to identity when its shape parameter goes to infinity, and (b) follows the CDF bound of a normalized Gamma RV [26]. Finally, through using binomial expansion, we obtain the tight approximation given in (10), and the proof is completed.

APPENDIX D

To further simplify (13), recall that the proposed protocol terminates image transmission as soon as $N_{\text{bg}} + N_{\text{roi}}$ fountain packets are correctly received at \mathcal{D} . Additionally, owing to the proposed semi-adaptive multi-packet transmission of public BG packets based on (7), which ensures all BG packets to be successfully delivered at \mathcal{D} , public transmission of BG packets is not faced with outage event. Consequently, if we denote the outage probability for the legitimate

link by Ω , we can model N_D^{out} as an RV following the negative binomial distribution $\mathcal{NB}(\frac{N_{\text{roi}}}{L_s}; \Omega)$, with the PMF given by

$$f_{N_D^{\text{out}}}(k) = \Pr(N_D^{\text{out}} = k) = \binom{\frac{N_{\text{roi}}}{L_s} + k - 1}{k} \Omega^k (1 - \Omega)^{\frac{N_{\text{roi}}}{L_s}}, k \geq 0, \quad (31)$$

where Ω can be derived as

$$\Omega = \Pr\left(\frac{BT}{b} \log_2(1 + \gamma_D^s) < L_s \mid \Psi_1\right) \stackrel{(a)}{=} \frac{\mathbf{1}_{(\theta \geq \kappa_s \nu)}}{\Pr(\Psi_1)} \left(\gamma(n_{\text{T}}, \frac{\theta}{\kappa_s}) - \gamma(n_{\text{T}}, \nu) \right) / \Gamma(n_{\text{T}}), \quad (32)$$

with (a) following from [33, Eq. (3.382.5)]. Therefore, based on (13), (31), and (32), by substituting $N_D^{\text{out}} = k - \tilde{N}$ in (31), (16) is obtained.

APPENDIX E

By assuming the fact that $T_E = \frac{N_{\text{roi}}}{L_s} + N_E^{\text{out}}$ and similar to the procedure of deriving (16), one can deduce that T_E has the following PMF, denoted by $f_{T_E}(k)$.

$$f_{T_E}(k) = \binom{k-1}{k - \frac{N_{\text{roi}}}{L_s}} \Lambda_c^{k - \frac{N_{\text{roi}}}{L_s}} (1 - \Lambda_c)^{\frac{N_{\text{roi}}}{L_s}}, k \geq \frac{N_{\text{roi}}}{L_s}, \quad (33)$$

where $c \in \{\text{NCE}, \text{CE}\}$. We remark that for Eves, we have assumed that the accumulation of N_{roi} confidential packets will suffice to intercept the image; hence, N_E^{out} represents the number of TSs that the public packets have been sent by \mathcal{S} , or the confidential packets have not been correctly recovered at wiretappers. Accordingly, for the NCE case we have

$$\begin{aligned} \Lambda_{\text{NCE}} &= \Pr(\Psi_1) \Pr\left\{ BT \log_2(1 + \gamma_E^{\text{NCE}}) < R \mid \Psi_1 \right\} + \Pr(\Psi_0) \\ &\stackrel{(a)}{=} \Pr(\Psi_1) \exp\left(-\beta \lambda_E (\zeta P_s / \theta)^{\frac{2}{\eta}} \left(1 + \frac{1/\zeta - 1}{n_{\text{T}} - 1} \theta\right)^{1 - n_{\text{T}}}\right) + \Pr(\Psi_0), \end{aligned} \quad (34)$$

where (a) follows from Lemma 1. Similarly, for the CE scenario, we can rewrite

$$\begin{aligned} \Lambda_{\text{CE}} &= \Pr(\Psi_1) \Pr\left\{ BT \log_2(1 + \gamma_E^{\text{CE}}) < R \mid \Psi_1 \right\} + \Pr(\Psi_0) \\ &\stackrel{(b)}{=} \Pr(\Psi_1) \left[1 - \sum_{k=0}^K \binom{K}{k} (-1)^k \mathcal{L}_{\gamma_E^{\text{CE}}}\left(\frac{k\varphi}{\theta}\right) \right] + \Pr(\Psi_0), \end{aligned} \quad (35)$$

with (b) following from Lemma 2, and $\mathcal{L}_{\gamma_E^{\text{CE}}}(\cdot)$ derived in (11).

REFERENCES

- [1] F. Hu, Y. Deng, W. Saad, M. Bennis, and A. H. Aghvami, "Cellular-connected wireless virtual reality: Requirements, challenges, and solutions," *IEEE Commun. Mag.*, vol. 58, no. 5, pp. 105–111, May 2020.
- [2] W. Saad, M. Bennis, and M. Chen, "A vision of 6G wireless systems: Applications, trends, technologies, and open research problems," *IEEE Network*, vol. 34, no. 3, pp. 134–142, May 2020.
- [3] A. Chorti, A. N. Barreto, S. Kopsell, M. Zoli, M. Chafii, P. Sehier, G. Fettweis, and H. V. Poor, "Context-aware security for 6G wireless The role of physical layer security," 2021, *arXiv:2101.01536*. [Online]. Available: <https://arxiv.org/abs/2101.01536>.
- [4] X. Li, C. Guo, L. Gupta, and R. Jain, "Efficient and secure 5G core network slice provisioning based on VIKOR approach," *IEEE Access*, vol. 7, pp. 150517–150529, Oct. 2019.
- [5] Y. Lu and L. D. Xu, "Internet of Things (IoT) cybersecurity research: A review of current research topics," *IEEE Internet of Things J.*, vol. 6, no. 2, pp. 2103–2115, Apr. 2019.
- [6] N. Wang, P. Wang, A. Alipour-Fanid, L. Jiao and K. Zeng, "Physical-layer security of 5G wireless networks for IoT: Challenges and opportunities," *IEEE Internet Things J.*, vol. 6, no. 5, pp. 8169–8181, Oct. 2019.
- [7] M. Letafati, A. Kuhestani, K. -K. Wong and M. J. Piran, "A lightweight secure and resilient transmission scheme for the Internet-of-Things in the presence of a hostile jammer," *IEEE Internet of Things J.*, Sep. 2020, doi: 10.1109/JIOT.2020.3026475.
- [8] D. He, C. Liu, H. Wang and T. Q. S. Quek, "Learning-based wireless powered secure transmission," *IEEE Wireless Commun. Lett.*, vol. 8, no. 2, pp. 600–603, Apr. 2019.
- [9] K. -L. Besser, P. -H. Lin, C. R. Janda, and E. A. Jorswieck, "Wiretap code design by neural network autoencoders," *IEEE Trans. Inf. Forensics Secur.*, vol. 15, pp. 3374–3386, Oct. 2019.
- [10] M. Jankowski, D. Gündüz, and K. Mikołajczyk, "Wireless image retrieval at the edge," *IEEE J. Sel. Areas Commun.*, vol. 39, no. 1, pp. 89–100, Jan. 2021.
- [11] Y. Lee and W. Tsai, "A new secure image transmission technique via secret-fragment-visible mosaic images by nearly reversible color transformations," *IEEE Trans. Circuits Syst. Video Technol.*, vol. 24, no. 4, pp. 695–703, Apr. 2014.
- [12] M. Letafati, A. Kuhestani, and H. Behroozi, "Three-hop untrusted relay networks with hardware imperfections and channel estimation errors for Internet of Things," *IEEE Trans. Inf. Forensics Secur.*, vol. 15, pp. 2856–2868, Mar. 2020.
- [13] M. Letafati, A. Kuhestani, H. Behroozi and D. W. K. Ng, "Jamming-resilient frequency hopping-aided secure communication for Internet-of-Things in the presence of an untrusted relay," *IEEE Trans. on Wireless Commun.*, vol. 19, no. 10, pp. 6771–6785, Oct. 2020.
- [14] M. Letafati, A. Kuhestani, D. W. Kwan Ng and M. R. Ahmadi Beshkani, "Physical layer secrecy and transmission resiliency of device-to-device communications," *GLOBECOM 2020 - 2020 IEEE Global Communications Conference*, Taipei, Taiwan, 2020, pp. 1–6.
- [15] C. Han, L. Sun and Q. Du, "Securing image transmissions via fountain coding and adaptive resource allocation," *2016 IEEE 83rd Vehicular Technology Conference (VTC Spring)*, Nanjing, 2016, pp. 1-5.
- [16] L. Sun, D. Huang and A. Lee Swindlehurst, "Fountain-coding aided secure transmission with delay and content awareness," *IEEE Trans. on Veh. Technol.*, vol. 69, no. 7, pp. 7992–7997, Jul. 2020.
- [17] L. Sun and H. Xu, "Fountain-coding-based secure communications exploiting outage prediction and limited feedback," *IEEE Trans. Veh. Technol.*, vol. 68, no. 1, pp. 740-753, Jan. 2019.
- [18] L. Sun, P. Ren, Q. Du, and Y. Wang, "Fountain-coding aided strategy for secure cooperative transmission in industrial wireless sensor networks," *IEEE Trans. Ind. Informat.*, vol. 12, no. 1, pp. 291-300, Feb. 2016.

- [19] H. Niu, M. Iwai, K. Sezaki, L. Sun, and Q. Du, "Exploiting fountain codes for secure wireless delivery," *IEEE Commun. Lett.*, vol. 18, no. 5, pp. 777–780, May 2014.
- [20] E. Bourtsoulatze, D. Burth Kurka, and D. Gündüz, "Deep joint source-channel coding for wireless image transmission," *IEEE Trans. Cogn. Commun. Netw.*, vol. 5, no. 3, pp. 567–579, Sep. 2019.
- [21] T. Marchioro, N. Laurenti, and D. Gündüz, "Adversarial networks for secure wireless communications," *ICASSP 2020 - 2020 IEEE International Conference on Acoustics, Speech and Signal Processing (ICASSP)*, Barcelona, Spain, 2020, pp. 8748–8752.
- [22] W. Guo, H. Zhao and Y. Tang, "Testbed for cooperative jamming cancellation in physical layer security," *IEEE Wireless Commun. Lett.*, vol. 9, no. 2, pp. 240–243, Feb. 2020.
- [23] X. Chen, D. W. K. Ng, W. Yu, E. G. Larsson, N. Al-Dhahir, and R. Schober, "Massive access for 5G and beyond," *IEEE J. Sel. Areas Commun.*, vol. 39, no. 3, pp. 615–637, Mar. 2021.
- [24] D. Stoyan, W. Kendall, and J. Mecke, *Stochastic Geometry and its Applications*, 2nd ed. John Wiley and Sons, 1996.
- [25] Y. Ju, H. Wang, T. Zheng, Q. Yin, and M. H. Lee, "Safeguarding millimeter wave communications against randomly located eavesdroppers," *IEEE Trans. Wireless Commun.*, vol. 17, no. 4, pp. 2675–2689, Apr. 2018.
- [26] T. Bai and R. W. Heath, "Coverage and rate analysis for millimeter-wave cellular networks," *IEEE Trans. Wireless Commun.*, vol. 14, no. 2, pp. 1100–1114, Feb. 2015.
- [27] I. Goodfellow, Y. Bengio, and A. Courville, *Deep Learning*. Cambridge, MA, USA: MIT Press, 2016.
- [28] M. Leshno, V. Y. Lin, A. Pinkus, and S. Schocken, "Multilayer feedforward networks with a nonpolynomial activation function can approximate any function," *Neural Netw.*, vol. 6, pp. 861–867, 1993.
- [29] B. Matthiesen, A. Zappone, K. -L. Besser, E. A. Jorswieck, and M. Debbah, "A globally optimal energy-efficient power control framework and its efficient implementation in wireless interference networks," *IEEE Trans. Signal Process.*, vol. 68, pp. 3887–3902, Jun. 2020.
- [30] D.P. Kingma and L.J. Ba, "Adam: A method for stochastic optimization," *2015 International Conference on Learning Representations (ICLR)*, San Diego, May 2015, pp. 1–13.
- [31] K. Deep, K. P. Singh, M. L. Kansal, and C. Mohan, "A real coded genetic algorithm for solving integer and mixed integer optimization problems," *Applied Mathematics and Computation*, vol. 212, pp. 505–518, Jun. 2009.
- [32] M. K. Simon and M.-S. Alouini, *Digital Communications over Fading Channels: A Unified Approach to Performance Analysis*. John Wiley, Inc., 2004.
- [33] I. S. Gradshteyn and I. M. Ryzhik, *Table of Integrals, Series, and Products*, 7th ed. New York: Academic, 2007.
- [34] *MATLAB® Parallel Computing Toolbox™*, MathWorks Inc. (2020), Natick, MA, USA, [Online]. Available: <https://www.mathworks.com/products/parallel-computing>.